Ann. Geophys. Discuss., https://doi.org/10.5194/angeo-2018-80
Manuscript under review for journal Ann. Geophys.
Discussion started: 6 July 2018

Annales Geophysicae Discussions
Open Access
EGU

On the variability of the semidiurnal solar and lunar tides of the equatorial electrojet during sudden stratospheric warmings

Tarique A. Siddiqui[1], Astrid Maute[1], Nick Pedatella[1], Yosuke Yamazaki[2], Hermann Lühr[2], and Claudia Stolle[2,3]

[1]High Altitude Observatory, National Center for Atmospheric Research, Boulder, CO, USA
[2]GFZ German Research Centre for Geosciences, Potsdam, Germany
[3]Faculty of Science, University of Potsdam, Germany

Correspondence: Tarique A. Siddiqui (tarique@ucar.edu)

Abstract. The variabilities of the semidiurnal solar and lunar tide of the equatorial electrojet (EEJ) are investigated during the 2003, 2006, 2009 and 2013 major sudden stratospheric warming (SSW) events in this study. For this purpose, the ground-magnetometer recordings at the equatorial observatories in Huancayo and Fuquene are utilized. Results show a major enhancement in the amplitude of the EEJ semidiurnal lunar tide in each of the four warming events. The EEJ semidiurnal solar tidal amplitude shows an amplification prior to the onset of warmings, a reduction during the deceleration of the zonal mean zonal wind at 60°N and 10 hPa and a second enhancement a few days after the peak reversal of the zonal mean zonal wind during all the four SSWs. Results also reveal that the amplitude of the EEJ semidiurnal lunar tide becomes comparable or even greater than the amplitude of the EEJ semidiurnal solar tide during all these warming events. The present study also compares the EEJ semidiurnal solar and lunar tidal changes with numerical simulations of the variability of the migrating semidiurnal solar (SW2) and lunar (M2) tide in neutral temperature at ∼120 km altitude. A better agreement between the enhancements of the EEJ semidiurnal lunar tide and the M2 tide in neutral temperature is observed in comparison with the enhancements of the EEJ semidiurnal solar tide and the SW2 tide in neutral temperature.

1 Introduction

Sudden stratospheric warming (SSW) events are large-scale winter-time polar meteorological phenomena, which usually occur in the Northern Hemisphere. These events are marked by a reversal of the climatological westerly zonal mean zonal winds in the polar stratosphere and a sudden increase in the polar stratospheric temperature by several tens of degrees (e.g., Andrews et al., 1987). SSWs result due to the breaking of amplified planetary waves propagating up from the troposphere and their interaction with the stratospheric zonal mean flow (e.g., Matsuno, 1971). These amplified planetary waves deposit momentum in the easterly direction in the polar stratosphere that results in the deceleration of the zonal mean zonal wind and also induces a mean meridional circulation (e.g., Haynes et al., 1991), which leads to an enhanced downwelling in the polar region and an increase in the polar stratospheric temperature due to adiabatic heating. As a result of SSWs, the polar vortex is generally observed to get either displaced off the pole or split into two vortices (e.g., Charlton and Polvani, 2007). SSWs can be classified into major and minor warming events based on the extent of deceleration of the zonal mean zonal wind at 60°N and 10 hPa

Ann. Geophys. Discuss., https://doi.org/10.5194/angeo-2018-80
Manuscript under review for journal Ann. Geophys.
Discussion started: 6 July 2018

Annales Geophysicae Discussions

pressure level. SSWs which only involve a deceleration of the zonal mean zonal winds at these levels without a complete reversal are termed as minor warmings and in cases where the zonal mean zonal winds get reversed are termed as major warmings.

The SSW-induced effects are not only limited to the polar stratosphere but are rather observed across many different regions of the atmosphere (e.g., Pedatella et al., 2018a). The warming in the polar stratosphere is accompanied by a cooling in the equatorial stratosphere (e.g., Fritz and Soules, 1970). In the mesosphere, the SSWs lead to cooling at polar latitudes (e.g., Labitzke, 1972; Liu and Roble, 2002) and warming at the equatorial latitudes (e.g., Garcia, 1987; Chandran and Collins, 2014). In the Southern Hemisphere, the SSW related effects lead to warming in the mesosphere through inter-hemispheric coupling mechanisms (e.g., Karlsson et al., 2009; Körnich and Becker, 2010). Coincident with the occurrence of SSWs, observations and modeling results have reported about the lower thermospheric warming at middle and polar latitudes (e.g., Liu and Roble, 2002; Goncharenko and Zhang, 2008; Funke et al., 2010). In the ionosphere, evidence of impact of SSWs at equatorial and low-latitudes have been reported in the form of enhanced semi-diurnal perturbations in vertical plasma drift velocities (e.g., Chau et al., 2009), total electron content (e.g., Goncharenko et al., 2010), electron densities (e.g., Lin et al., 2013) and the equatorial electrojet (e.g., Vineeth et al., 2009; Fejer et al., 2010; Yamazaki et al., 2012). These perturbations have mainly been attributed to the modulation of the atmospheric solar and lunar tides during SSWs (e.g., Chau et al., 2012; Pedatella and Liu, 2013).

Atmospheric tides are global-scale oscillations of the atmosphere with periods and sub-periods of a solar or a lunar day (Lindzen and Chapman, 1969). The lower atmospheric solar tides are forced thermally through periodic absorption of solar radiation by stratospheric ozone and tropospheric water vapour while the atmospheric lunar tides are mainly gravitationally forced. The solar and lunar tides generated in the lower atmospheric regions propagate vertically upward and on reaching the dynamo region heights drive ionospheric currents (e.g., Baker et al., 1953). One such current flow as a result of this wind driven dynamo is the EEJ. It is a narrow ribbon of intense current flowing above the dip equator in the E-region of the ionosphere (e.g., Chapman, 1951). It is a daytime phenomenon and confined to a latitudinal width of about $\pm 3^{\circ}$. The zonal polarization electric fields that drive the EEJ are generated by the ionospheric wind dynamo mechanism (e.g., Heelis, 2004) and the intense current in the EEJ is the result of the Cowling effect (Cowling, 1932) at the magnetic equator.

The variations in the EEJ due to solar and lunar tidal changes during SSWs have been a widely studied topic in recent years. However, the evidence of large changes in the EEJ during Northern Hemisphere winters due to the modulation of atmospheric lunar tides has been known since the work of Bartels and Johnston (1940). They noticed the occurrence of occasional 'big-L days' usually during December-February, when anomalously enhanced lunar tidal variations accompanied by counter-electrojets are observed in the horizontal component of the magnetic field. Although Bartels and Johnston (1940) didn't link the occurrence of 'big-L days' to SSWs; in recent years a renewed interest in this topic has been generated following the works of Chau et al. (2009) and Fejer et al. (2010). They identified a conspicuous semidiurnal signature that shifts in time on succeeding days in the F-region vertical plasma drifts and in the EEJ during the SSW events. Fejer et al. (2010) suggested that this signature in the EEJ could be linked to the enhancements of the lunar semidiurnal tide (M2). Since then, a number of studies have confirmed their findings using magnetic observations from satellite (e.g., Park et al., 2012) and ground-based observatories

Ann. Geophys. Discuss., https://doi.org/10.5194/angeo-2018-80
Manuscript under review for journal Ann. Geophys.
Discussion started: 6 July 2018

Annales Geophysicae Discussions

(e.g., Yamazaki et al., 2012; Yamazaki, 2013; Sathishkumar and Sridharan, 2013; Siddiqui et al., 2017; Yadav et al., 2017). Numerical and observational studies (e.g., Liu et al., 2010; Fuller-Rowell et al., 2010; Jin et al., 2012; Pedatella et al., 2014) have concluded that the solar semidiurnal tide (SW2) at the mesosphere and thermosphere altitudes also gets enhanced during SSWs. A number of mechanisms have been proposed in recent years to explain the changes in the atmospheric semidiurnal tides during SSWs. The SW2 may be amplified during SSWs due to changes in the distribution of ozone (e.g., Goncharenko et al., 2012; Sridharan et al., 2012), changes in the tidal propagation conditions (e.g., Jin et al., 2012) and interaction with the enhanced planetary waves (e.g., Liu et al., 2010). The reason for amplification of the M2 is explained by the shifting of the secondary atmospheric resonance peak on the lunar semidiurnal period (e.g., Forbes and Zhang, 2012). The variabilities of the solar and lunar tides of the EEJ have been studied during the 2006 and the 2009 SSW events using the Indian magnetometer stations by Sathishkumar and Sridharan (2013) and enhancements in both the solar and lunar semidiurnal tides of the EEJ were reported. Yamazaki (2014) estimated the relative importance of the solar and lunar current systems and found that the absolute changes in solar and lunar current systems are comparable during SSWs.

In this study, we use the data from the Huancayo and Fuquene magnetic observatories to examine the EEJ solar and lunar semidiurnal tidal enhancements during the 2003, 2006, 2009 and 2013 major SSW events. The main purpose of this paper is to investigate the temporal evolution of the semidiurnal solar and lunar tidal amplitude enhancement relative to the reversal of the zonal mean zonal wind at 60°N and 10 hPa. Model simulations of the 2009 SSW event (e.g., Jin et al., 2012; Fang et al., 2012; Pedatella et al., 2014), in particular, have shown an enhancement in the amplitude of SW2 in the lower thermosphere prior to the onset of SSW, followed by a reduction during the deceleration of zonal mean zonal wind at 60°N and 10hPa and then another enhancement of SW2 after the peak reversal of the zonal mean zonal wind. We further investigate if the semidiurnal solar tide of the EEJ also shows a similar variability during the SSWs as seen in the SW2 from modeling results. The outline of the paper is as follows. Section 2 describes the data sets used in this study. In section 3, the analysis methods used for determining the EEJ solar and lunar tidal amplitudes are described. Section 4 presents the observations which is followed by discussion in section 5 and the conclusions in section 6.

2 Data Set

The hourly mean values of the horizontal component of the geomagnetic field at Huancayo (-12.05° N, 284.67°E; magnetic latitude: -0.6°) and Fuquene (5.47°N, 286.26°E; magnetic latitude: 18.12°) are downloaded from the World Data Centre (WDC) for Geomagnetism, Edinburgh. Daily solar flux ($F_{10.7}$) values (Tapping, 2013) are downloaded from the GSFC/SPDF OMNIWeb interface at http://omniweb.gsfc.nasa.gov. The night-time baseline values of the magnetic field are estimated using the five monthly International Quiet Days (IQD) which are downloaded from the website of German Research Centre for Geosciences (GFZ), Potsdam.

The SSW events are identified by following the World Meteorological Organization (WMO) definition of an SSW. For this purpose, daily mean values of the North Pole temperature at 10 hPa and the zonal wind at 60°N and 10 hPa are obtained

Ann. Geophys. Discuss., https://doi.org/10.5194/angeo-2018-80
Manuscript under review for journal Ann. Geophys.
Discussion started: 6 July 2018

Annales Geophysicae Discussions

from the National Centers for Environmental Prediction/National Center of Atmospheric Research (NCEP/NCAR) reanalysis datasets (Kalnay et al., 1996).

3 Methods of Analysis

3.1 Estimating the EEJ strength from ground-magnetometer recordings

The strength of EEJ is estimated by using the horizontal component of the ground-magnetometer recordings at Huancayo (HUA) and Fuquene (FUQ). The locations of the two observatories are marked in Figure 1. The difference of the horizontal magnetic fields between an observatory located under the EEJ and another located outside of the EEJ can be used to estimate the strength of EEJ (Rastogi and Klobuchar, 1990). The steps for this calculation have been described in detail for the HUA and FUQ observatories in Siddiqui et al. (2015b) and are only briefly summarized here in the following paragraph.

For both the observatories, the mean of the night-time values between 23:30-02:30 LT are obtained using the five monthly International Quiet Days. The quiet night-time values are used to approximate the magnetic effects of the Earth's main field. Thereafter, these values are subtracted from the recorded magnetic data at both the observatories and the daily variation with respect to the night-time baseline values are computed. The large-scale fields due to the magnetospheric ring current and the solar quiet (Sq) current systems are removed when the difference between the horizontal magnetic fields of the two observatories are calculated (e.g., Manoj et al., 2006). On computing this difference, the hourly values of the EEJ strength are obtained. The EEJ values also show a strong dependence on the solar flux levels (e.g., Alken and Maus, 2007). To minimize this dependence, the estimated EEJ strength has been normalized to a solar flux level of 150 s.f.u using the method described in Park et al. (2012).

3.2 Estimating the solar and lunar tidal variations of the EEJ

The dominant tidal components of the EEJ are the solar (S) diurnal (24 hours) and semidiurnal (12 hrs) variations. In addition, the EEJ also contains lunar (L) tidal variations, which mostly result due to the lunar semidiurnal (12.42 hours, M2) tidal component. The amplitude of L in the EEJ is typically an order of magnitude less than the amplitude of S but occasionally the amplitude of L can become comparable to the S amplitude on certain 'big-L days' (Bartels and Johnston, 1940), which are usually observed during the Northern Hemisphere winters. Recent studies have suggested that these days with enhanced lunar tidal effects are related to the occurrence of SSW events (e.g., Fejer et al., 2010; Siddiqui et al., 2015a).

In this study, the S and L variations of the EEJ are determined by using the methods described in Malin and Chapman (1970). Although the main focus of their study was determination of the lunar daily variations in geophysical quantities using the Chapman-Miller method, however, they have also described the method for determining the solar daily variations in geophysical quantities. The lunar and solar daily variations of the EEJ are mathematically expressed as follows:

The components of the L variations are represented by the Chapman's phase law and can be expressed as -

$$L_n = l_n \, sin(\frac{2\pi}{24} nt - \frac{2\pi}{24} 2\nu + \lambda_n) \quad (1)$$

Ann. Geophys. Discuss., https://doi.org/10.5194/angeo-2018-80
Manuscript under review for journal Ann. Geophys.
Discussion started: 6 July 2018

Annales Geophysicae Discussions

where l_n denotes the amplitude of the nth component of the L variations, t denotes the solar in hours, ν denotes the lunar age in hours and λ_n is the phase angle of the nth component.

The components of S variations can be expressed as:

$$S_n = s_n\, sin(\frac{2\pi}{24}nt + \sigma_n) \tag{2}$$

where s_n and σ_n denote the amplitude and phase of the nth harmonic component, respectively.

The L and S variations are estimated by determining their four respective Fourier coefficients through least-squares fitting of the normalized EEJ values by using the following expressions:

$$L = \sum_{n=1}^{4} l_n\, sin(\frac{2\pi}{24}nt - \frac{2\pi}{24}2\nu + \lambda_n) \tag{3}$$

$$S = \sum_{n=1}^{4} s_n\, sin(\frac{2\pi}{24}nt + \sigma_n) \tag{4}$$

The L variations of the EEJ are essentially semidiurnal because of the dominance of the L_2 term and the L variations are modified by other harmonics in a way such that it is smaller during the night than the day (Malin and Chapman, 1970). It is important to keep note of this point because the EEJ signals are absent during the night-time. Conte et al. (2017) showed that a window size of length greater than 15 days is sufficient to resolve the solar and lunar semidiurnal tides in mesosphere-lower thermosphere (MLT) winds in a similar least-squares fitting approach. For this study, we use a 21-day moving window, which is moved forward by 1 day, for the least-squares fitting in order to better resolve the lunar and solar tidal components. We assume constant amplitude and phase of the tidal components within the 21-day window.

4 Observations and Results

In this section, we examine the day-to-day variabilities of the EEJ, the polar stratospheric conditions and the semidiurnal solar (S_2) and lunar (L_2) tidal variations during the 2002-2003, 2005-2006, 2008-2009 and 2012-2013 major SSWs.

4.1 2002-2003 SSW event

Figure 2a presents the normalized daily EEJ values, which have been scaled up to 150 s.f.u, between December 1, 2002 and March 1, 2003. The days of new and full moon are represented by open and filled circles, respectively. Figure 2b shows the L_2 (blue line) and S_2 (red line) tidal amplitudes. Figure 2c shows the zonal mean zonal wind (U) at 60°N and 10 hPa (red line) pressure level and the North Pole temperature (T) also at the 10 hPa (black line) pressure level. Figure 2e presents the $F_{10.7}$ levels during this time interval. The onset of this SSW event begins during the final week of December and the characteristic increase in the temperature at the North Pole and the reversal of the zonal mean zonal wind is witnessed later in January. During 28th to 31st December, the EEJ (Fig 2a) weakens in the morning hours and counter-electrojets are observed in the afternoon

Ann. Geophys. Discuss., https://doi.org/10.5194/angeo-2018-80
Manuscript under review for journal Ann. Geophys.
Discussion started: 6 July 2018

Annales Geophysicae Discussions

hours. Coinciding with the occurrence of the new moon, which occurs on the 2nd of January, the semidiurnal perturbation pattern in the EEJ during SSWs increasingly shifts in local time on succeeding days. The amplification of the L_2 and the S_2 amplitudes (Fig 2b) happen during this period, with the lunar tidal amplification clearly being the more dominant among the two. The L_2 amplitude increases by up to a factor of 2 compared to pre-SSW levels while the S_2 amplitude shows only a minor enhancement during this time interval. In Figure 2b, the upper and lower boundaries of the shaded regions represent the 1 σ uncertainty level. The amplitude of L_2 reaches a peak value of 29 nT on 5th January and the S_2 amplitude reaches a peak value of 25 nT also on the same day. After this enhancement the S_2 amplitude starts to decrease and reaches a minimum value of 14 nT on 21st January. A second weaker perturbation pattern in EEJ starts after the day of the full moon on 18th January. The zonal mean zonal wind reaches a greater level of reversal during this period but a similar enhancement in the L_2 amplitude is not observed. A second enhancement in the S_2 amplitude is seen to start after the minima on 21st January and reaches a peak value of 24 nT on 2nd February. The L_2 amplitude, in the meantime, declines and reaches its pre-SSW levels.

Figures 2d and 2f present the phase variation of the S_2 and L_2, respectively. The phase of S_2 remains stable at around 10 h (LT) in the pre- and post-SSW periods. It starts to get slightly perturbed during the onset of the SSW moving to earlier times and reaches a minimum of 8.8 h (LT) on January 1, 2003. Thereafter, it increases gradually and reaches the pre-SSW levels. The error bars in these figures denote the 1σ uncertainty level. The phase of L_2 on the other hand shows the expected progressive shift between 6-17 LT and no major perturbations in the L_2 phase are observed due to this SSW event. At the cross-over points of the L_2 and S_2 phases stronger EEJs are expected due to the constructive interference between the L_2 and S_2 tidal components. Equivalently, S_2 and L_2 wave troughs overlap typically around 15-16 LT on days shortly after the new and full moon. Zhou et al. (2018) found high occurrence rates of CEJ during that time span around December solstice.

4.2 2005-2006 SSW event

From Figure 3c, it is observed that the onset of the 2005-2006 SSW starts in the first week of January and this event witnesses multiple episodes of warming with the North Pole temperature peaking on the 4th, 11th and 23rd January. In Figure 3a, between 10th to 13th January, the EEJ weakens and counter-electrojet events are recorded after 10 h (LT). The shifting semidiurnal perturbation pattern in the EEJ starts to evolve from 14th January coinciding with the occurrence of full moon and the EEJ shows enhanced morning and weakened afternoon amplitudes. The reversal of the zonal mean zonal wind at 60°N and 10 hPa is first witnessed on 22nd January and the peak wind reversal occurs on 26th January. The EEJ again weakens between 26th-28th January prior to the appearance of a second perturbation pattern, which coincides with the occurrence of new moon. The solar flux levels, shown in Figure 3e, remains below 100 s.f.u. during this SSW event.

In Figure 3b, the amplitude of the S_2 (red line) and L_2 (blue line) tidal variations are presented. The upper and lower boundaries of shaded regions again represent the 1 σ uncertainty level. The L_2 amplitude shows a sharp increase from 7nT on 31st December to 28nT on 13th January during the onset of SSW. It is approximately maintained at these levels till 22nd January before a sharp decline to pre-SSW levels is seen in February. The S_2 amplitude on the other hand gets enhanced just before the onset of SSW with the peak amplitude of 27nT being recorded on 25th December. Thereafter, it shows a decline

Ann. Geophys. Discuss., https://doi.org/10.5194/angeo-2018-80
Manuscript under review for journal Ann. Geophys.
Discussion started: 6 July 2018

Annales Geophysicae Discussions

following the start of SSW and decreases to 15nT on 10th January. The S_2 amplitude is then again seen to enhance towards the end of January.

In Figure 3d, the phase of S_2 is presented. Like the case of the 2003 SSW event, the phase remains fairly constant between 9-10 h (LT) before the onset of SSW event. It then decreases to 7.8 h (LT) during the SSW before returning to pre-SSW levels. In Figure 3f, the phase of L_2 shows its characteristic propagation in solar local time.

4.3 2008-2009 SSW event

The onset of the 2009 SSW can be observed to start in the second week of January from Figure 4c. The North Pole temperature doesn't show major fluctuations during this period but a sudden decrease in the zonal mean zonal wind speed is seen to begin from 11th January. The enhancement in the North Pole temperature first starts on 19th January and then reaches a peak on 23rd January. The zonal mean zonal wind speed, meanwhile, continues to decelerate and shows a reversal on 24th January followed by a minima on 29th January. From Figure 4a, it is observed that during the onset of this SSW event the EEJ amplitudes first get weakened between 21st to 25th January and after the occurrence of the new moon on 26th January, the progressing semidiurnal perturbation pattern in the EEJ is again witnessed. The 2009 SSW event was recorded during the minimum phase of the solar cycle and the solar flux levels (Fig 4e) was extremely low.

In Figure 4b, the amplitude of the L_2 (blue line) starts increasing with the onset of SSW and reaches a peak amplitude of 31nT on 29th January. The L_2 amplitude then starts to decline when the zonal mean zonal wind starts to recover and approximately reaches the pre-SSW levels. The tidal characteristics of the S_2 (red line) amplitudes are similar to the ones seen during the 2003 and 2006 SSW events. An earlier enhancement is observed at the onset of SSW followed by a decline during the main phase of SSW and then another enhancement is observed following the peak zonal mean zonal wind reversal. In the 2009 SSW event, the first peak enhancement of S_2 is observed on 5th January with a peak amplitude of 36 nT and once the SSW moves into its main phase the S_2 amplitude declines to a minimum of 21 nT on 20th January. Following the peak wind reversal, the S_2 amplitude gets enhanced to 40 nT in the first week of February.

The phase of S_2, as seen in Figure 4d, shows a gradual increase in the month of December and peaks during the onset of SSW. In the main phase of SSW, there is a decline in the tidal phase from 10 h (LT) to 8.5 h (LT) and then the tidal phase returns back to its pre-SSW levels in February. Using the Whole Atmosphere Model (WAM), Fuller-Rowell et al. (2010) also found similar changes in the phase of SW2 tide at $\sim$110 km at Northern Hemisphere mid-latitudes during the 2009 SSW event. They suggested that the phase change in SW2 is due to the change in propagation conditions of the atmosphere due to the SSWs. As the S_2 tidal variations of the EEJ is mainly driven by the SW2 tide originating from below, modeling results of Fuller-Rowell et al. (2010) and our observations suggest that the changes in the phase of SW2 tide due to modified atmospheric conditions during SSWs could also be causing the changes in the phase of S_2. Unlike the S_2 phase, the L_2 phase, seen in Figure 4f, shows only minor perturbations during the 2009 SSW event and its characteristic propagation pattern is again well observed.

Ann. Geophys. Discuss., https://doi.org/10.5194/angeo-2018-80
Manuscript under review for journal Ann. Geophys.
Discussion started: 6 July 2018

Annales Geophysicae Discussions

4.4 2012-2013 SSW event

From the North Pole temperature and the zonal mean zonal wind data in Figure 5c, the onset of this SSW event begins at the start of January. The North Pole temperature shows enhancement from 2nd January and reaches its peak value on 6th January. In the meantime, the zonal mean zonal wind amplitude starts to decelerate and then gets reversed on 7th January. Thereafter it decelerates again and reaches a peak reversal on 19th January. The EEJ amplitudes (Figure 6a), as seen in the earlier SSWs, first get weakened between 8th to 10th January and after the new moon on 11th January starts to display the semidiurnal perturbation pattern. This pattern then evolves on succeeding days and can be more clearly observed between 15th to 20th January. The discontinuous variation and CEJ on 17th Jan could be related to enhanced geomagnetic activity on that day. Zhou et al. (2018) have shown that CEJ can be caused by enhancement of geomagnetic activity levels. The reduction of the EEJ amplitudes prior to the enhanced semidiurnal pattern is similar to the observations of equatorial vertical drifts reported in Maute et al. (2015). In their work, they used the numerical simulation results for the 2013 SSW event to show that the amplitude of equatorial vertical drifts gets reduced during this event due to the phenomenon of beats between the enhanced SW2 and M2 tides. The similar periods of SW2 and M2 will produce a theoretical beating frequency of 1/(15.13 day) and in Figure 6a, we can observe that the days with reduced EEJ amplitudes, on either side of the enhanced semidiurnal pattern, are separated by a similar time period. As the EEJ and vertical plasma drifts are driven by the daytime eastward polarization electric fields it is likely that the weakening of EEJ amplitudes is being caused due to the beating phenomenon between the enhanced SW2 and M2 tides.

From Figure 5b, two episodes of the L_2 enhancements can be observed. The first enhancement starts in the second week of December and a peak tidal amplitude of 19 nT is estimated on 28th December. A stronger second enhancement starts on 6th January and a peak tidal amplitude of 27 nT is then estimated on 15th January. The S_2 enhancements also start in the same period and the peak amplitude of 41 nT is recorded on 7th January. The S_2 amplitude then shows a slight decrease during the main phase of SSW and reaches a minimum value of 31 nT on 31st January. Thereafter it again shows an enhancement and reaches an amplitude of 37 nT on 9th February. Compared to the three previous SSW events, the S_2 amplitude decreases more gradually and shows the smallest reduction during the main phase of this SSW event.

The phase of S_2 (Fig 5d), once again shows a slight decrease at the onset and during the SSW event as in the case of the three previous SSWs. The phase again stabilizes following the peak reversal of the zonal mean zonal wind during this event. The phase of the L_2 seems to be consistent with the expected propagating phase pattern in solar time. The solar flux levels for this event, seen in Figure 5e, range from moderate to high levels between December to February with peak values around 160 s.f.u being recorded during the main phase of SSW.

5 Discussion

The S_2 and L_2 variations of the EEJ during SSWs obtained from ground-magnetometer observations are compared with variations of the SW2 and M2 tides in neutral temperature at $\sim$120 km in this section. The simulation results, which are

Ann. Geophys. Discuss., https://doi.org/10.5194/angeo-2018-80
Manuscript under review for journal Ann. Geophys.
Discussion started: 6 July 2018

Annales Geophysicae Discussions

available for the 2003, 2009 and 2013 SSW events, are utilized for this purpose. In addition, the possible mechanisms that could be responsible for the observed S_2 and L_2 variability of the EEJ during SSWs are discussed.

For the 2002-2003 SSW event, the results from the National Center for Atmospheric Research Whole Atmosphere Community Climate Model eXtended version with "Specified Dynamics" (SD-WACCMX) (Liu et al., 2018) are used to investigate the SW2 variability. The simulations are forced with the NASA Modern-Era Retrospective Analysis for Research and Applications (MERRA) reanalysis from 0-50 km. Figure 6 depicts the SW2 tide in neutral temperature at ∼120 km altitude. The SW2 tide in zonal winds at this altitude could also have been shown in the figures and a similar variability in the SW2 tidal amplitudes should be expected. A moving window of 21 day length is used for the estimation of the SW2 tidal amplitude and phase. The SW2 amplitude shows prominent amplification at mid-latitudes in both the hemispheres during this SSW event. The hemispherical asymmetry in SW2 enhancements is noticeable, which could be due to the hemispheric differences in the tidal propagation conditions that result in excitation of asymmetric tidal modes (e.g., Forbes et al., 2013). The SW2 amplitude (Figure 6a) at the mid-latitudes in the Southern Hemisphere (SH) shows relatively stronger enhancements between days 6-21 and 36-41. In the Northern Hemisphere (NH), the enhancements at mid-latitudes are more prominent between days 34-38. SW2 maxima of ∼25 K is recorded in the SH on day 9, while in the NH the peak amplitude is ∼15 K on day 36. To a certain degree, there is a similarity in timing between the enhancements of the SW2 and the S_2 over Huancayo (Figure 2b) between days 34-40. The maxima in SW2 is seen at low- and mid-latitudes in both the hemispheres during this time interval. The S_2 enhancements in the first week of January coincides more with the SW2 enhancements in the SH during this time interval. However, the reduction of S_2 following the first enhancement does not exactly correspond to the reduction of SW2 amplitudes during this event. Based on the presented analysis, we conclude that the day to day variation of S_2 amplitude during the 2003 SSW cannot be fully explained by the day to day variation of SW2 tidal amplitude obtained from simulation results at dynamo region heights for this event.

For the 2008-2009 SSW event, we use the simulations described in Pedatella et al. (2018b) to investigate the thermospheric SW2 and M2 tidal amplification. The modeling output was obtained using the Whole Atmosphere Community Climate Model eXtended version (WACCMX) (see Liu et al. (2018) for details) in which the lower and middle atmosphere variability was constrained using the Data Assimilation Research Testbed (DART) ensemble adjustment Kalman filter. In this simulation, an additional M2 forcing term is included in the model physics (Pedatella et al., 2012). The SW2 and M2 tides in neutral temperature at ∼120 km altitude are depicted in Figure 7. A moving window of 21 day length is used to separate the solar and lunar semidiurnal tides. The SW2 amplitude at midlatitudes in SH shows an enhancement in Figure 7a between days 1 and 5 followed by a reduction between days 15 and 20 and a second enhancement between days 20 and 40. In the NH, the SW2 enhancement is only prominent between days 20 and 40. The M2 enhancements can be observed in Figure 7c between days 10-20 and days 25-35. The M2 amplitudes show a hemispherical asymmetry with the peak values occurring in the NH. The timing of the first S_2 enhancement of the EEJ (Figure 4b) and its reduction is seen to coincide with the SW2 amplitudes in the SH. The timing of the second SW2 enhancement that is seen in both the hemispheres also shows a good agreement with the S_2 enhancements over Huancayo. Compared to the 2003 SSW event, the SW2 amplitude for the 2009 SSW event shows a better agreement with the EEJ S_2 enhancements. On comparing the amplification of the M2 amplitude in neutral temperature and the

Ann. Geophys. Discuss., https://doi.org/10.5194/angeo-2018-80
Manuscript under review for journal Ann. Geophys.
Discussion started: 6 July 2018

L_2 at Huancayo (Figure 4b), it is observed that the enhancements are simultaneous and the peak amplification is achieved on day 29 in both the cases.

For the 2012-2013 SSW, the SW2 and M2 tides are investigated using the modeling results of Maute et al. (2015). In their work, the NCAR thermosphere-ionosphere-mesosphere-electrodynamics general circulation (TIME-GCM) model was used to study the modulation of the daytime equatorial vertical drift due to this SSW event. Figure 8 depicts the SW2 and M2 tides in neutral temperature at ∼120 km altitude. This result is consistent with the findings of Maute et al. (2015). In Figure 8a, the SW2 tidal amplitudes are presented and the hemispheric asymmetry in SW2 enhancements is once again noticeable. The SW2 tidal amplification in the SH is seen at mid-latitudes all throughout January while in the Northern Hemisphere the SW2 amplification at mid-latitudes starts only after 10th January. The peak amplification occurs simultaneously in both the hemispheres on 23rd January. The M2 tidal amplification seen in Figure 8c also shows hemispherical asymmetry, with the amplitudes in the SH being almost twice as large as in the NH. The M2 amplitudes get enhanced between 10th to 20th January and its peak value is seen on 16th January in both the hemispheres. The comparison between the timing of M2 enhancements in neutral temperature and the L_2 at Huancayo (Figure 5b), shows that they coincide with each other, which is not exactly the case with the solar semidiurnal enhancements. The peak SW2 enhancements in neutral temperature occur a few days later than the S_2 enhancements over Huancayo. The semidiurnal tidal amplitudes in neutral temperature for the 2013 SSW event is comparably larger than the other two SSW events and absolute comparison in semidiurnal tidal amplitudes between the three SSWs should be avoided. The difference exists due to the different models that are used to produce the simulation output. The tidal amplitudes in WACCM-X are known to be damped (e.g., Pedatella et al., 2018b) in order to stabilize the model.

The modeling results of the 2009 (Pedatella et al., 2018b) and the 2013 (Maute et al., 2015) SSWs were able to reproduce the $E \times B$ drifts from observations for these two SSW events and therefore it is not unreasonable to compare the EEJ semidiurnal tidal enhancements with the semidiurnal tidal enhancments in neutral temperature. From the simulation and observation results, we find that the timing of the M2 amplification in neutral temperature and the L_2 amplification in the EEJ show a better agreement with each other compared to the amplification of SW2 in neutral temperature and the S_2 in the EEJ during the 2009 and 2013 SSWs. It is also important to note that the peak enhancements in M2 and L_2 occur on the same day during these two events. The mechanism of the M2 enhancement during SSWs has been explained by Forbes and Zhang (2012) through the shifting of the so-called Pekeris resonance peak of the atmosphere to the M2 lunar period. The location of the resonance peak shifts due to the changes in the zonal mean temperature and wind structure of the middle atmosphere during SSWs. The enhanced M2 amplitudes at dynamo region heights drive an enhanced lunar current system in the ionosphere during SSWs (Yamazaki, 2014) and would lead to an enhancement of L_2 variations in the EEJ.

The asymmetrical SW2 enhancements during the 2003, 2009 and 2013 SSWs suggest that the asymmetrical tidal modes are important for understanding the SW2 tidal variability during SSWs. Jin et al. (2012) used the Ground-to-topside model of Atmosphere and Ionosphere for Aeronomy (GAIA) to investigate the SW2 Hough modes, which were decomposed from the neutral temperature at 116 km altitude, during the 2009 SSW event and found the largest temporal variations in the symmetric semidiurnal (2,2) and the asymmetric semidiurnal (2,3) modes (Jin et al., 2012, see Figure 9). The enhancement of asymmetric solar tidal modes also cause major changes in the structure of the ionospheric solar current systems during SSWs (Yamazaki,

Ann. Geophys. Discuss., https://doi.org/10.5194/angeo-2018-80
Manuscript under review for journal Ann. Geophys.
Discussion started: 6 July 2018

Annales Geophysicae Discussions

2014). However, as the wavelength of the asymmetric solar tidal modes at dynamo region heights are much smaller than the symmetric solar tidal modes (e.g., Stening, 1969; Tarpley, 1970; Stening, 1989), their effectiveness in generating currents in the ionosphere are smaller than the symmetrical tidal modes (Stening, 1969). The EEJ solar tidal changes during SSWs is therefore more likely to be caused due to the variability of the symmetrical solar tidal modes. This could be one of the reasons for the lack of agreement between the SW2 tidal enhancements in neutral temperature and S_2 of the EEJ.

To explain the changes in the SW2 at the mesospheric and thermospheric altitudes due to SSWs, a number of mechanisms have been proposed through both observation and modeling studies. Pedatella and Forbes (2010) investigated the 2009 SSW event and suggested that the changing mean wind conditions in the MLT during the SSW and post-SSW period could be a reason for the reduction and enhancement of the SW2 amplitudes in GPS TEC observations. Wang et al. (2011) proposed the nonlinear wave-wave interactions of migrating solar diurnal (DW1), semidiurnal (SW2) and terdiurnal (TW3) tides as the reason for the decrease of SW2 amplitude in the ionospheric E-region during the 2009 SSW event. It was suggested by them that the DW1, SW2 and TW3 form a resonant triad and a direct wave-wave interaction among these tides may lead to a rapid growth in one of the tide at the expense of other two. Based on their results, they concluded that the SW2 tide was losing energy to the TW3 tide, resulting in the amplification of the latter during the 2009 SSW. The TW3 tidal amplification during the 2009 SSW event was also confirmed in the results of Fuller-Rowell et al. (2010) and Fang et al. (2012). The SW2 amplitudes in the MLT and upper thermosphere may also be affected by the redistribution of ozone during SSWs (e.g., Goncharenko et al., 2012; Sridharan et al., 2012). In case of the 2009 SSW event, Goncharenko et al. (2012) noted that the ozone levels in the tropical stratosphere increased immediately after the SSW and due to increased solar tidal forcing this could have possibly led to the enhancement of the SW2 tide as ozone is a major excitation source of the SW2 tide (e.g., Lindzen and Chapman, 1969). Modeling study by Jin et al. (2012) proposed that the changes in the structure of the zonal mean zonal wind and the meridional temperature gradient in the middle atmosphere during SSWs lead to a change in the tidal propagation conditions and could result in amplification of the SW2 tide in the MLT and upper thermosphere.

Numerical study by McLandress (2002) showed that the amplitude of the DW1 in the MLT can get amplified if there is an enhancement of the meridional wind shear in the upper atmosphere. A meridional shear in the eastward (westward) direction in the NH broadens (narrows) the tropical waveguide of the tides. Sassi et al. (2013) used this hypothesis to show that the decrease in the amplitude of the SW2 tide have resulted due to the increase in the westward meridional shear in the MLT during the 2009 SSW event. Another mechanism that has been proposed to explain the SW2 tidal changes during SSWs is the nonlinear tide-wave interaction between the stationary planetary waves and SW2 (Liu et al., 2010). Simulation results of the 2006 SSW event by Maute et al. (2014) confirmed an increase in SW1 and a decrease in SW2 in the E-region due to the non-linear tide wave interactions between the SW2 and planetary wave number 1 during this event.

It is likely that a combination of the above-mentioned mechanisms are responsible for the observed SW2 variability at ionospheric altitudes. The SSW-induced changes in the SW2 drive the variability in the S_2 of the EEJ during SSWs through the ionospheric dynamo mechanism. The global reduction and amplification in the SW2 amplitudes during the SSWs as seen at ionospheric altitudes is therefore also reflected in the S_2 variations of the EEJ. However, more research would be needed for completely understanding the role of symmetrical and asymmetrical solar tidal modes in causing the solar tidal variability of

EEJ during SSWs. In addition, the relative importance of the mechanisms responsible for the changes in SW2 during SSWs also needs to be studied.

6 Conclusions

In this study, we have used the ground-magnetic field recordings at the Huancayo and Fuquene observatories to determine the semidiurnal solar and lunar tidal variability of the EEJ during the 2003, 2006, 2009 and 2013 major SSWs. The solar and lunar tidal variabilities are then compared with the timing of the occurrence of the SSWs. Major conclusions derived from this study are as follows.

1. The semidiurnal lunar tide of the EEJ shows major amplification during all the four SSW events and its amplitude is observed to become comparable or even greater than the semidiurnal solar tide. In addition, the relative amplification of the EEJ lunar semidiurnal tide is seen to be larger than the EEJ solar semidiurnal tide during all the four SSWs.

2. The EEJ semidiurnal solar tidal amplitude shows enhancement prior to the onset of the SSWs, which is then followed by a reduction during the deceleration of the zonal mean zonal wind and then a subsequent enhancement when the zonal mean zonal wind starts to recover after its peak reversal.

3. The timing of the global M2 enhancements in neutral temperature at $\sim$120 km and the EEJ semidiurnal lunar tidal enhancements during SSWs show a good agreement with each other. In case of a similar comparison between the SW2 and the EEJ semidiurnal solar tidal enhancements, the degree of agreement varies for each of the SSW events.

Competing interests. The authors declare that they have no competing interests.

Acknowledgements. We would like to thank the Instituto Geofisico del Peru and Instituto Geográfico Agustin Codazzi, Colombia for supporting geomagnetic observatory operations at Huancayo and Fuquene, respectively. The F10.7 data are obtained from NASA GSFC/SPDF OMNIWeb. The NCEP-NCAR reanalysis data are available at the NOAA/OAR/ESRL website. The list of International Quiet Days are available from GFZ Potsdam. C.S and H.L are partly supported by SPP 1788 “Dynamic Earth" of the Deutsche Forschungsgemeinschaft (DFG). Y.Y was supported by the Humboldt Research Fellowship for Experienced Researchers from the Alexander von Humboldt Foundation. The National Center for Atmospheric Research is sponsored by National Science Foundation. T.A.S and A.M are supported by NASA grant X13AF77G.

References

Alken, P. and Maus, S.: Spatio-temporal characterization of the equatorial electrojet from CHAMP, Ørsted, and SAC-C satellite magnetic measurements, Journal of Geophysical Research: Space Physics (1978–2012), 112, https://doi.org/10.1029/2007JA012524, 2007.

Andrews, D. G., Holton, J. R., and Leovy, C. B.: Middle atmosphere dynamics, 40, Academic press, 1987.

Baker, W., Martyn, D. F., et al.: Electric currents in the ionosphere-The conductivity, Phil. Trans. R. Soc. Lond. A, 246, 281–294, 1953.

Bartels, J. and Johnston, H.: Geomagnetic tides in horizontal intensity at Huancayo, Terrestrial Magnetism and Atmospheric Electricity, 45, 269–308, https://doi.org/10.1029/TE045i003p00269, 1940.

Chandran, A. and Collins, R.: Stratospheric sudden warming effects on winds and temperature in the middle atmosphere at middle and low latitudes: a study using WACCM., Annales Geophysicae (09927689), 32, 2014.

Chapman, S.: The equatorial electrojet as detected from the abnormal electric current distribution above Huancayo, Peru, and elsewhere, Meteorology and Atmospheric Physics, 4, 368–390, https://doi.org/10.1007/BF02246814, 1951.

Charlton, A. J. and Polvani, L. M.: A new look at stratospheric sudden warmings. Part I: Climatology and modeling benchmarks, Journal of Climate, 20, 449–469, https://doi.org/10.1175/JCLI3996.1, 2007.

Chau, J., Fejer, B. G., and Goncharenko, L.: Quiet variability of equatorial E x B drifts during a sudden stratospheric warming event, Geophysical Research Letters, 36, https://doi.org/10.1029/2008GL036785, 2009.

Chau, J. L., Goncharenko, L. P., Fejer, B. G., and Liu, H.-L.: Equatorial and Low Latitude Ionospheric Effects During Sudden Stratospheric Warming Events, Space Science Reviews, 168, 385–417, https://doi.org/10.1007/s11214-011-9797-5, 2012.

Conte, J. F., Chau, J. L., Stober, G., Pedatella, N., Maute, A., Hoffmann, P., Janches, D., Fritts, D., and Murphy, D. J.: Climatology of semidiurnal lunar and solar tides at middle and high latitudes: Interhemispheric comparison, Journal of Geophysical Research: Space Physics, 122, 7750–7760, 2017.

Cowling, T. G.: The electrical conductivity of an ionised gas in the presence of a magnetic field, Monthly Notices of the Royal Astronomical Society, 93, https://doi.org/10.1093/mnras/93.1.90, 1932.

Fang, T.-W., Fuller-Rowell, T., Akmaev, R., Wu, F., Wang, H., and Anderson, D.: Longitudinal variation of ionospheric vertical drifts during the 2009 sudden stratospheric warming, Journal of Geophysical Research: Space Physics, 117, https://doi.org/10.1029/2011JA017348, a03324, 2012.

Fejer, B. G., Olson, M. E., Chau, J. L., Stolle, C., Lühr, H., Goncharenko, L. P., Yumoto, K., and Nagatsuma, T.: Lunar-dependent equatorial ionospheric electrodynamic effects during sudden stratospheric warmings, Journal of Geophysical Research: Space Physics, 115, https://doi.org/10.1029/2010JA015273, a00G03, 2010.

Forbes, J. M. and Zhang, X.: Lunar tide amplification during the January 2009 stratosphere warming event: Observations and theory, Journal of Geophysical Research: Space Physics (1978–2012), 117, https://doi.org/10.1029/2012JA017963, 2012.

Forbes, J. M., Zhang, X., Bruinsma, S., and Oberheide, J.: Lunar semidiurnal tide in the thermosphere under solar minimum conditions, Journal of Geophysical Research: Space Physics, 118, 1788–1801, 2013.

Fritz, S. and Soules, S.: Large-scale temperature changes in the stratosphere observed from Nimbus III, Journal of the Atmospheric Sciences, 27, 1091–1097, 1970.

Fuller-Rowell, T., Wu, F., Akmaev, R., Fang, T.-W., and Araujo-Pradere, E.: A whole atmosphere model simulation of the impact of a sudden stratospheric warming on thermosphere dynamics and electrodynamics, Journal of Geophysical Research: Space Physics, 115, 2010.

Funke, B., López-Puertas, M., Bermejo-Pantaleón, D., García-Comas, M., Stiller, G. P., von Clarmann, T., Kiefer, M., and Linden, A.: Evidence for dynamical coupling from the lower atmosphere to the thermosphere during a major stratospheric warming, Geophysical Research Letters, 37, https://doi.org/10.1029/2010GL043619, l13803, 2010.

Garcia, R. R.: On the mean meridional circulation of the middle atmosphere, Journal of the atmospheric sciences, 44, 3599–3609, 1987.

Goncharenko, L. and Zhang, S.-R.: Ionospheric signatures of sudden stratospheric warming: Ion temperature at middle latitude, Geophysical Research Letters, 35, https://doi.org/10.1029/2008GL035684, l21103, 2008.

Goncharenko, L. P., Coster, A. J., Chau, J. L., and Valladares, C. E.: Impact of sudden stratospheric warmings on equatorial ionization anomaly, Journal of Geophysical Research: Space Physics, 115, https://doi.org/10.1029/2010JA015400, a00G07, 2010.

Goncharenko, L. P., Coster, A. J., Plumb, R. A., and Domeisen, D. I. V.: The potential role of stratospheric ozone in the stratosphere-ionosphere coupling during stratospheric warmings, Geophysical Research Letters, 39, https://doi.org/10.1029/2012GL051261, 2012.

Haynes, P. H., McIntyre, M. E., Shepherd, T. G., Marks, C. J., and Shine, K. P.: On the “Downward Control" of Extratropical Diabatic Circulations by Eddy-Induced Mean Zonal Forces, Journal of the Atmospheric Sciences, 48, 651–678, https://doi.org/10.1175/1520-0469(1991)048<0651:OTCOED>2.0.CO;2, 1991.

Heelis, R.: Electrodynamics in the low and middle latitude ionosphere: A tutorial, Journal of Atmospheric and Solar-Terrestrial Physics, 66, 825–838, 2004.

Jin, H., Miyoshi, Y., Pancheva, D., Mukhtarov, P., Fujiwara, H., and Shinagawa, H.: Response of migrating tides to the stratospheric sudden warming in 2009 and their effects on the ionosphere studied by a whole atmosphere-ionosphere model GAIA with COSMIC and TIMED/SABER observations, Journal of Geophysical Research: Space Physics, 117, https://doi.org/10.1029/2012JA017650, 2012.

Kalnay, E., Kanamitsu, M., Kistler, R., Collins, W., Deaven, D., Gandin, L., Iredell, M., Saha, S., White, G., Woollen, J., Zhu, Y., Chelliah, M., Ebisuzaki, W., Higgins, W., Janowiak, J., Mo, K. C., Ropelewski, C., Wang, J., Leetmaa, A., Reynolds, R., Jenne, R., and Joseph, D.: The NCEP/NCAR 40-Year Reanalysis Project, Bulletin of the American Meteorological Society, 77, 437–472, https://doi.org/10.1175/1520-0477(1996)077<0437:TNYRP>2.0.CO;2, 1996.

Karlsson, B., McLandress, C., and Shepherd, T. G.: Inter-hemispheric mesospheric coupling in a comprehensive middle atmosphere model, Journal of Atmospheric and Solar-Terrestrial Physics, 71, 518–530, 2009.

Körnich, H. and Becker, E.: A simple model for the interhemispheric coupling of the middle atmosphere circulation, Advances in Space Research, 45, 661–668, 2010.

Labitzke, K.: Temperature Changes in the Mesosphere and Stratosphere Connected with Circulation Changes in Winter, Journal of the Atmospheric Sciences, 29, 756–766, https://doi.org/10.1175/1520-0469(1972)029<0756:TCITMA>2.0.CO;2, 1972.

Lin, C., Lin, J., Chang, L., Chen, W., Chen, C., and Liu, J.: Stratospheric sudden warming effects on the ionospheric migrating tides during 2008–2010 observed by FORMOSAT-3/COSMIC, Journal of Atmospheric and Solar-Terrestrial Physics, 103, 66–75, 2013.

Lindzen, R. S. and Chapman, S.: Atmospheric tides, Space science reviews, 10, 3–188, 1969.

Liu, H.-L. and Roble, R. G.: A study of a self-generated stratospheric sudden warming and its mesospheric–lower thermospheric impacts using the coupled TIME-GCM/CCM3, Journal of Geophysical Research: Atmospheres, 107, https://doi.org/10.1029/2001JD001533, 4695, 2002.

Liu, H.-L., Wang, W., Richmond, A. D., and Roble, R. G.: Ionospheric variability due to planetary waves and tides for solar minimum conditions, Journal of Geophysical Research: Space Physics, 115, https://doi.org/10.1029/2009JA015188, 2010.

Liu, H.-L., Bardeen, C. G., Foster, B. T., Lauritzen, P., Liu, J., Lu, G., Marsh, D. R., Maute, A., McInerney, J. M., Pedatella, N. M., et al.: Development and Validation of the Whole Atmosphere Community Climate Model With Thermosphere and Ionosphere Extension (WACCM-X 2.0), Journal of Advances in Modeling Earth Systems, 10, 381–402, 2018.

Malin, S. and Chapman, S.: The determination of lunar daily geophysical variations by the Chapman-Miller method, Geophysical Journal International, 19, 15–35, 1970.

Manoj, C., Lühr, H., Maus, S., and Nagarajan, N.: Evidence for short spatial correlation lengths of the noontime equatorial electrojet inferred from a comparison of satellite and ground magnetic data, Journal of Geophysical Research: Space Physics (1978–2012), 111, https://doi.org/10.1029/2006JA011855, 2006.

Matsuno, T.: A dynamical model of the stratospheric sudden warming, Journal of the Atmospheric Sciences, 28, 1479–1494, 1971.

Maute, A., Hagan, M., Richmond, A., and Roble, R.: TIME-GCM study of the ionospheric equatorial vertical drift changes during the 2006 stratospheric sudden warming, Journal of Geophysical Research: Space Physics, 119, 1287–1305, 2014.

Maute, A., Hagan, M. E., Yudin, V., Liu, H.-L., and Yizengaw, E.: Causes of the longitudinal differences in the equatorial vertical E × B drift during the 2013 SSW period as simulated by the TIME-GCM, Journal of Geophysical Research: Space Physics, 120, 5117–5136, https://doi.org/10.1002/2015JA021126, 2015JA021126, 2015.

McLandress, C.: The seasonal variation of the propagating diurnal tide in the mesosphere and lower thermosphere. Part II: The role of tidal heating and zonal mean winds, Journal of the Atmospheric Sciences, 59, 907–922, 2002.

Park, J., Lühr, H., Kunze, M., Fejer, B. G., and Min, K. W.: Effect of sudden stratospheric warming on lunar tidal modulation of the equatorial electrojet, Journal of Geophysical Research: Space Physics (1978–2012), 117, https://doi.org/10.1029/2011JA017351, 2012.

Pedatella, N., Liu, H.-L., and Richmond, A.: Atmospheric semidiurnal lunar tide climatology simulated by the whole atmosphere community climate model, Journal of Geophysical Research: Space Physics, 117, 2012.

Pedatella, N., Chau, J., Schmidt, H., Goncharenko, L., Stolle, C., Hocke, K., Harvey, V., Funke, B., and Siddiqui, T.: How Sudden Stratospheric Warming Affects the Whole Atmosphere, Eos, https://doi.org/10.1029/2018EO092441, 2018a.

Pedatella, N., Liu, H.-L., Marsh, D., Raeder, K., Anderson, J., Chau, J., Goncharenko, L., and Siddiqui, T.: Analysis and Hindcast Experiments of the 2009 Sudden Stratospheric Warming in WACCMX+ DART, Journal of Geophysical Research: Space Physics, 123, 3131–3153, 2018b.

Pedatella, N. M. and Forbes, J. M.: Evidence for stratosphere sudden warming-ionosphere coupling due to vertically propagating tides, Geophysical Research Letters, 37, https://doi.org/10.1029/2010GL043560, 2010.

Pedatella, N. M. and Liu, H.: The influence of atmospheric tide and planetary wave variability during sudden stratosphere warmings on the low latitude ionosphere, Journal of Geophysical Research: Space Physics, 118, 5333–5347, https://doi.org/10.1002/jgra.50492, 2013.

Pedatella, N. M., Fuller-Rowell, T., Wang, H., Jin, H., Miyoshi, Y., Fujiwara, H., Shinagawa, H., Liu, H.-L., Sassi, F., Schmidt, H., Matthias, V., and Goncharenko, L.: The neutral dynamics during the 2009 sudden stratosphere warming simulated by different whole atmosphere models, Journal of Geophysical Research: Space Physics, 119, 1306–1324, https://doi.org/10.1002/2013JA019421, 2014.

Rastogi, R. and Klobuchar, J.: Ionospheric electron content within the equatorial F2 layer anomaly belt, Journal of Geophysical Research: Space Physics, 95, 19 045–19 052, 1990.

Sassi, F., Liu, H.-L., Ma, J., and Garcia, R. R.: The lower thermosphere during the northern hemisphere winter of 2009: A modeling study using high-altitude data assimilation products in WACCM-X, Journal of Geophysical Research: Atmospheres, 118, 8954–8968, 2013.

Sathishkumar, S. and Sridharan, S.: Lunar and solar tidal variabilities in mesospheric winds and EEJ strength over Tirunelveli (8.7°N, 77.8°E) during the 2009 major stratospheric warming, Journal of Geophysical Research: Space Physics, 118, 533–541, https://doi.org/10.1029/2012JA018236, 2013.

Siddiqui, T. A., Lühr, H., Stolle, C., and Park, J.: Relation between stratospheric sudden warming and the lunar effect on the equatorial electrojet based on Huancayo recordings, Annales Geophysicae, 33, 235–243, https://doi.org/10.5194/angeo-33-235-2015, 2015a.

Siddiqui, T. A., Stolle, C., Lühr, H., and Matzka, J.: On the relationship between weakening of the northern polar vortex and the lunar tidal amplification in the equatorial electrojet, Journal of Geophysical Research: Space Physics, 120, 10 006–10 019, https://doi.org/10.1002/2015JA021683, 2015b.

Siddiqui, T. A., Stolle, C., and Lühr, H.: Longitude-dependent lunar tidal modulation of the equatorial electrojet during stratospheric sudden warmings, Journal of Geophysical Research: Space Physics, 122, 3760–3776, 2017.

Sridharan, S., Sathishkumar, S., and Gurubaran, S.: Variabilities of mesospheric tides during sudden stratospheric warming events of 2006 and 2009 and their relationship with ozone and water vapour, Journal of Atmospheric and Solar-Terrestrial Physics, 78, 108–115, 2012.

Stening, R.: An assessment of the contributions of various tidal winds to the Sq current system, Planetary and Space Science, 17, 889–908, 1969.

Stening, R. J.: A calculation of ionospheric currents due to semidiurnal antisymmetric tides, Journal of Geophysical Research: Space Physics, 94, 1525–1531, 1989.

Tapping, K.: The 10.7 cm solar radio flux (F10.7), Space Weather, 11, 394–406, 2013.

Tarpley, J. D.: The ionospheric wind dynamo-II. Solar tides, Planetary and Space Science, https://doi.org/10.1016/0032-0633(70)90110-8, 1970.

Vineeth, C., Kumar Pant, T., and Sridharan, R.: Equatorial counter electrojets and polar stratospheric sudden warmings - a classical example of high latitude-low latitude coupling?, Annales Geophysicae, 27, 3147–3153, https://doi.org/10.5194/angeo-27-3147-2009, 2009.

Wang, H., Fuller-Rowell, T., Akmaev, R., Hu, M., Kleist, D., and Iredell, M.: First simulations with a whole atmosphere data assimilation and forecast system: The January 2009 major sudden stratospheric warming, Journal of Geophysical Research: Space Physics, 116, 2011.

Yadav, S., Pant, T. K., Choudhary, R., Vineeth, C., Sunda, S., Kumar, K., Shreedevi, P., and Mukherjee, S.: Impact of Sudden Stratospheric Warming of 2009 on the Equatorial and Low-Latitude Ionosphere of the Indian Longitudes: A Case Study, Journal of Geophysical Research: Space Physics, 122, 2017.

Yamazaki, Y.: Large lunar tidal effects in the equatorial electrojet during northern winter and its relation to stratospheric sudden warming events, Journal of Geophysical Research: Space Physics, 118, 7268–7271, https://doi.org/10.1002/2013JA019215, 2013.

Yamazaki, Y.: Solar and lunar ionospheric electrodynamic effects during stratospheric sudden warmings, Journal of Atmospheric and Solar-Terrestrial Physics, 119, 138–146, 2014.

Yamazaki, Y., Richmond, A., and Yumoto, K.: Stratospheric warmings and the geomagnetic lunar tide: 1958–2007, Journal of Geophysical Research: Space Physics (1978–2012), 117, https://doi.org/10.1029/2012JA017514, 2012.

Zhou, Y.-L., Lühr, H., Xu, H.-W., and Alken, P.: Comprehensive analysis of the counter equatorial electrojet: Average properties as deduced from CHAMP observations, Journal of Geophysical Research: Space Physics, https://doi.org/10.1029/2018JA025526, 2018.

Ann. Geophys. Discuss., https://doi.org/10.5194/angeo-2018-80
Manuscript under review for journal Ann. Geophys.
Discussion started: 6 July 2018

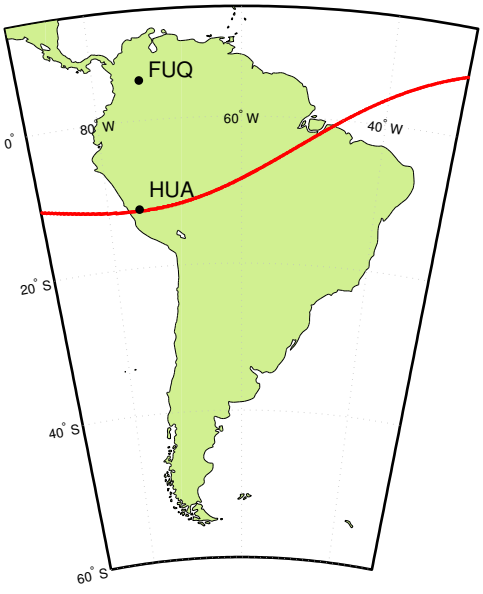

Figure 1. The locations of the Huancayo (HUA) and Fuquene (FUQ) observatory are marked in black dots in this figure. The red line denotes the dip equator.

Ann. Geophys. Discuss., https://doi.org/10.5194/angeo-2018-80
Manuscript under review for journal Ann. Geophys.
Discussion started: 6 July 2018

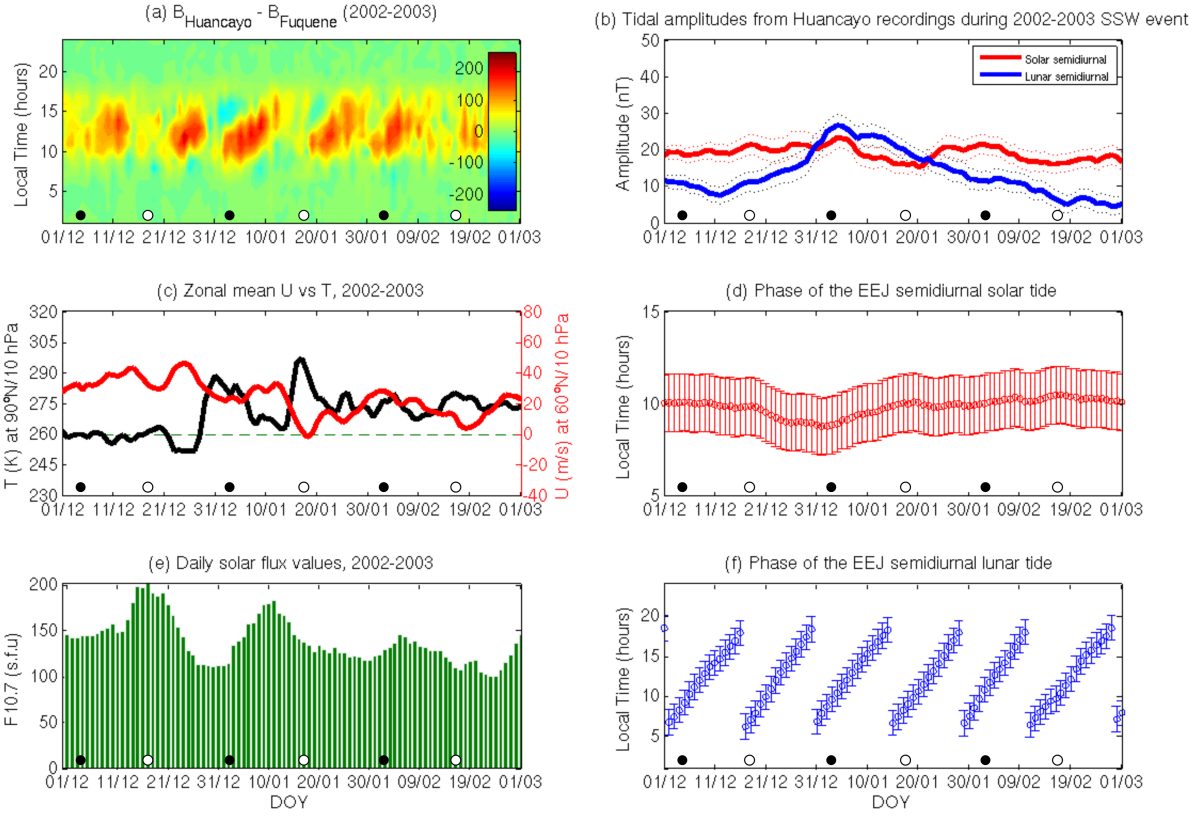

Figure 2. (a) The day-to-day variations of the EEJ obtained from Huancayo and Fuquene observatories between 1st December 2002 and 1st March 2003 are presented in this plot. The white and black dots at the bottom represent the days of full moon and new moon, respectively. (b) The amplitude of the semidiurnal solar (red) and lunar (blue) tide of the EEJ during the same period. The boundaries of the shaded regions represent the 1σ uncertainty level. (c) Daily time series of the zonal mean zonal wind (U) at 60°N and 10 hPa (red) and the North Pole temperature at 10 hPa (black) during the same period. The dashed green line is marked to identify the day of reversal of the zonal mean zonal wind. (d) The phase of the semidiurnal tide of the EEJ. (e) Daily solar flux values during this time interval. (f) The phase of the semidiurnal lunar tide of the EEJ.

Ann. Geophys. Discuss., https://doi.org/10.5194/angeo-2018-80
Manuscript under review for journal Ann. Geophys.
Discussion started: 6 July 2018

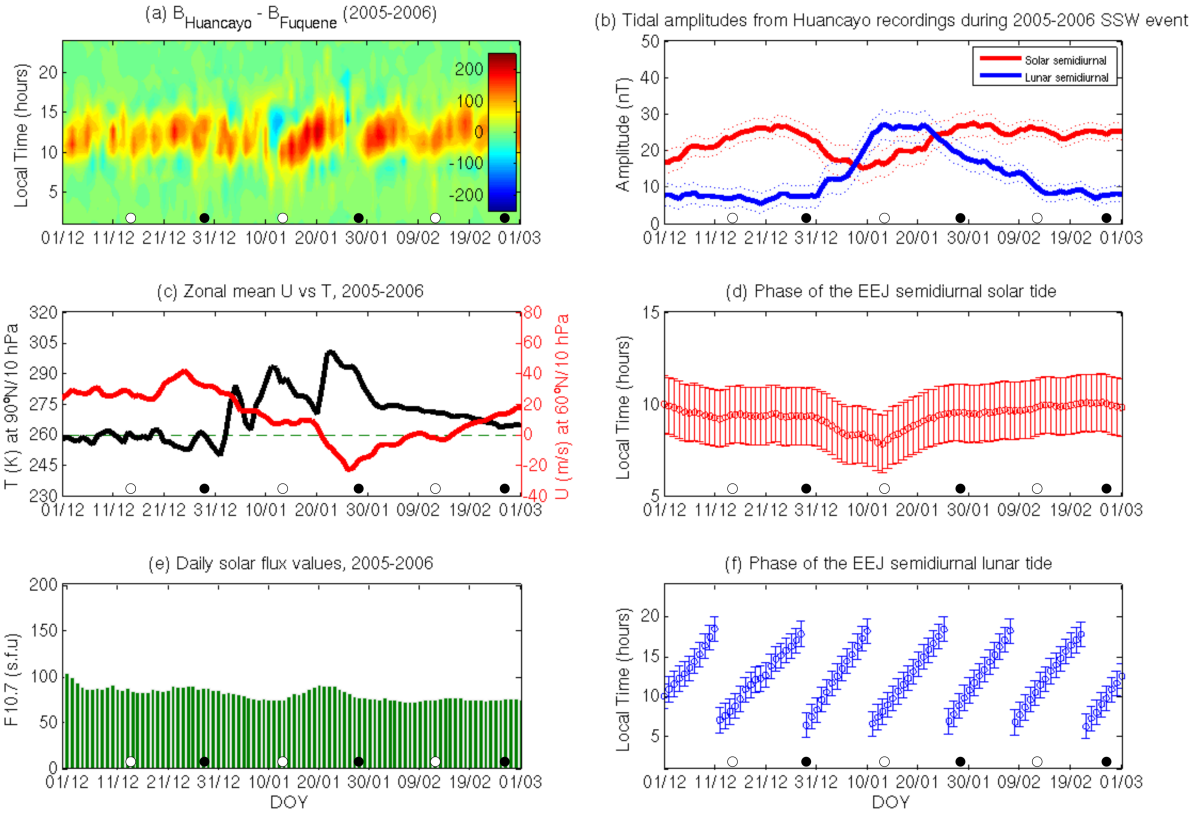

Figure 3. Same as Figure 2 except between 1st December 2005 and 1st March 2006

Ann. Geophys. Discuss., https://doi.org/10.5194/angeo-2018-80
Manuscript under review for journal Ann. Geophys.
Discussion started: 6 July 2018

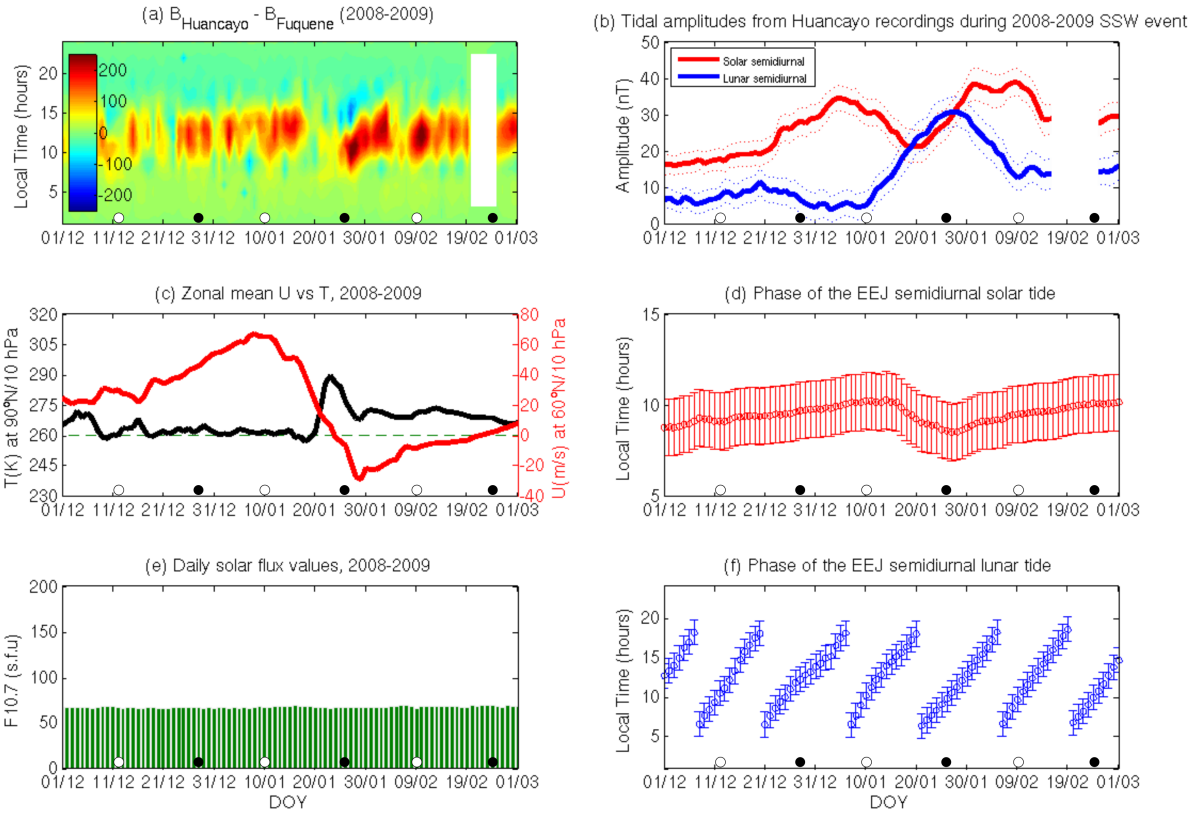

Figure 4. Same as Figure 2 except between 1st December 2008 and 1st March 2009

Ann. Geophys. Discuss., https://doi.org/10.5194/angeo-2018-80
Manuscript under review for journal Ann. Geophys.
Discussion started: 6 July 2018

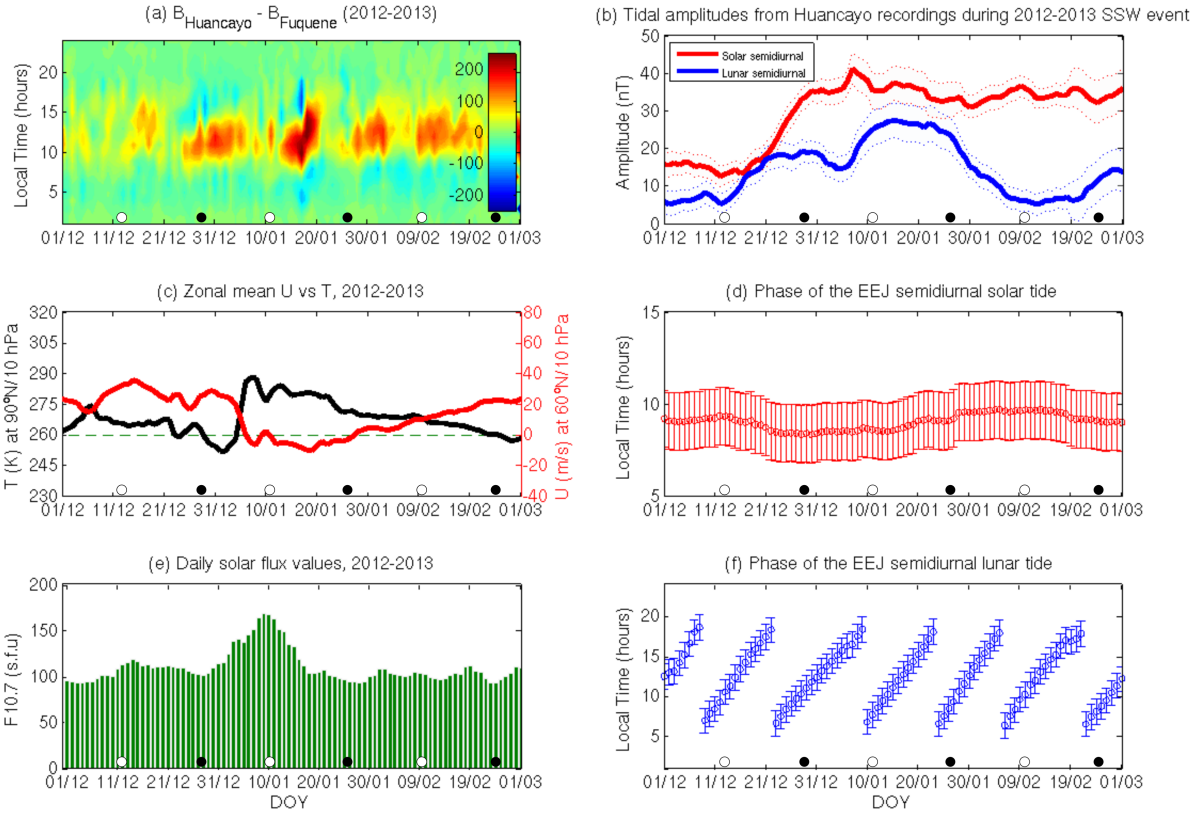

Figure 5. Same as Figure 2 except between 1st December 2012 and 1st March 2013

Ann. Geophys. Discuss., https://doi.org/10.5194/angeo-2018-80
Manuscript under review for journal Ann. Geophys.
Discussion started: 6 July 2018

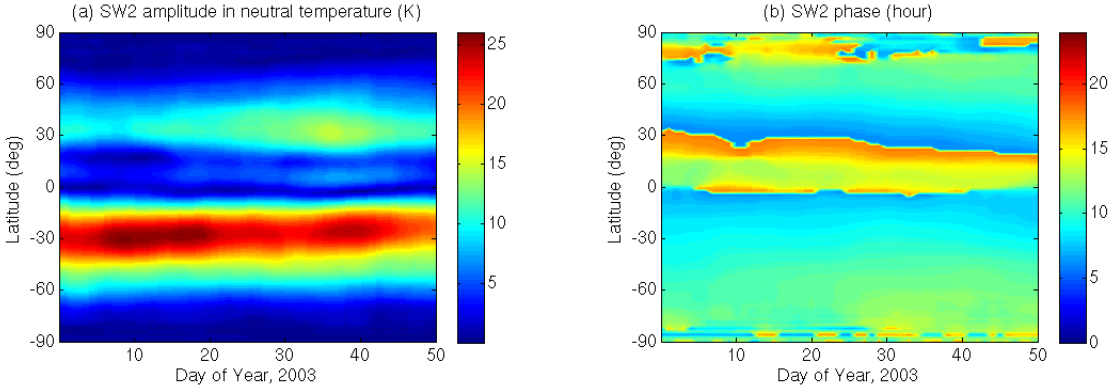

Figure 6. The amplitude (a) and phase (b) of the SW2 tide in neutral temperature at ∼120 km during the 2002-2003 SSW event.

Ann. Geophys. Discuss., https://doi.org/10.5194/angeo-2018-80
Manuscript under review for journal Ann. Geophys.
Discussion started: 6 July 2018

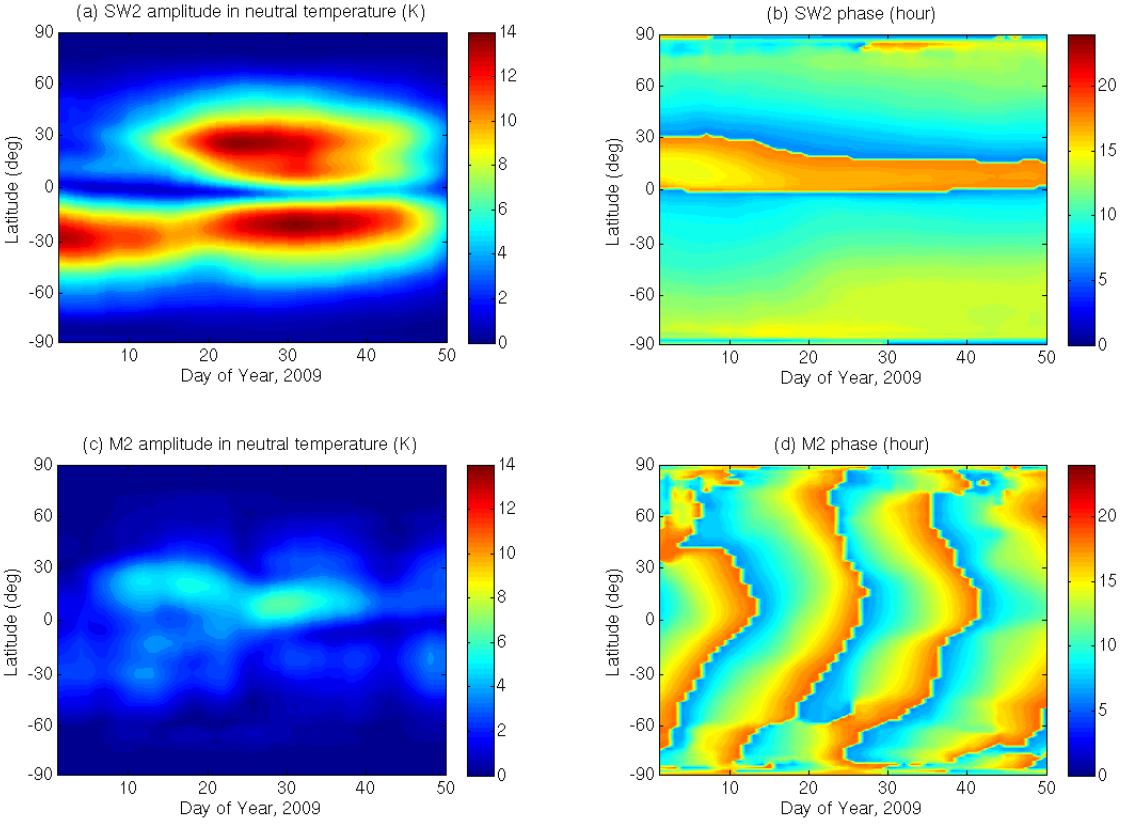

Figure 7. The amplitude (a) and phase (b) of the SW2 tide in neutral temperature at ∼ 120 km during the 2008-2009 SSW event (simulations from Pedatella et al., 2018a). The amplitude and phase of the M2 tide during the same period is presented in (c) and (d), respectively.

Ann. Geophys. Discuss., https://doi.org/10.5194/angeo-2018-80
Manuscript under review for journal Ann. Geophys.
Discussion started: 6 July 2018

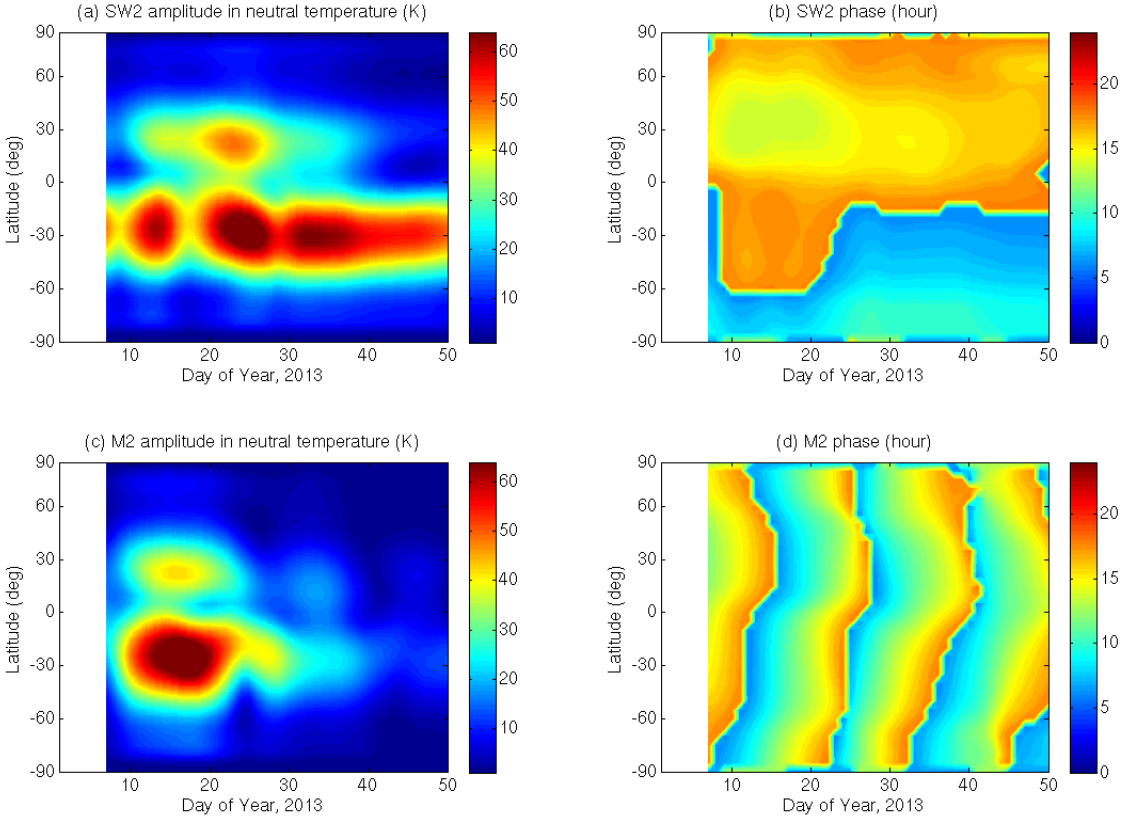

Figure 8. Same as Figure 7 except during the 2012-2013 SSW event (simulations from Maute et al., 2015).